NJC

New Journal of Chemistry

A journal for new directions in chemistry

Accepted Manuscript

This article can be cited before page numbers have been issued, to do this please use: L. Ma, J. Xu, L. Li, M. Mao and S. Zhao, *New J. Chem.*, 2020, DOI: 10.1039/D0NJ04021E.

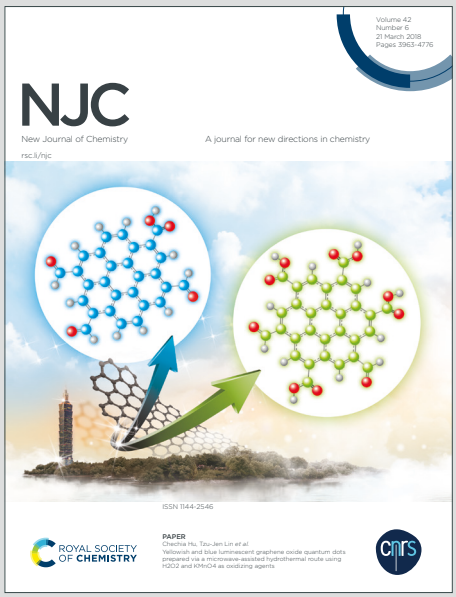

This is an Accepted Manuscript, which has been through the Royal Society of Chemistry peer review process and has been accepted for publication.

Accepted Manuscripts are published online shortly after acceptance, before technical editing, formatting and proof reading. Using this free service, authors can make their results available to the community, in citable form, before we publish the edited article. We will replace this Accepted Manuscript with the edited and formatted Advance Article as soon as it is available.

You can find more information about Accepted Manuscripts in the Information for Authors.

Please note that technical editing may introduce minor changes to the text and/or graphics, which may alter content. The journal's standard Terms & Conditions and the Ethical guidelines still apply. In no event shall the Royal Society of Chemistry be held responsible for any errors or omissions in this Accepted Manuscript or any consequences arising from the use of any information it contains.

Hydrothermal synthesis of WO_3/CoS_2 n-n heterojunction for Z-scheme photocatalytic H_2 evolution

Lijun Ma[1], Jing Xu*[1,2,3], Lingjiao Li[1], Min Mao[1], Sheng Zhao[1]

1. School of Chemistry and Chemical Engineering, North Minzu University, Yinchuan 750021, PR China.

2. Ningxia Key Laboratory of Solar Chemical Conversion Technology, North Minzu University, Yinchuan 750021, PR China.

3. Key Laboratory of Chemical Engineering and Technology, State Ethnic Affairs Commission, North Minzu University, Yinchuan 750021, PR China.

Corresponding author email: wgyxj2000@163.com

Abstract

One of the effective methods to improve electron transfer efficiency and photocatalytic reaction activity is to construct a photocatalyst with a heterojunction interface. This article synthesized WO_3/CoS_2 n-n heterojunction composite catalyst, the photocatalytic hydrogen evolution experiment was optimized by adjusting the pH of the triethanolamine solution, the amount of Eosin Y added and the content of WO_3 in the composite catalyst. After five hours of photocatalytic reaction, WO_3/CoS_2 (WCS-2) had a H_2 production of 221.15 μmol, which was 80.41 times that of single WO_3 and 2.17 times that of CoS_2, and had good stability. XRD, SEM, TEM and XPS characterization results indicated that WO_3/CoS_2 was successfully prepared. Fluorescence test and electrochemical test results showed that the WO_3/CoS_2 catalyst had a higher photoelectron transfer efficiency. Finally, it is pointed out that the WO_3/CoS_2 enhanced the photocatalytic activity, which may be due to the electron migration of WO_3 and CoS_2 following the Z-scheme mechanism. This work supplies a new idea for constructing n-n heterojunction to enhance the activity of photocatalytic hydrogen production.

Keywords: Photocatalyst; WO_3/CoS_2; n-n heterojunction; Z-scheme

1. Introduction

Due to people's extensive use of non-renewable energy sources such as petroleum, it has caused a string of environmental contamination and energy shortage problems [1,2]. Hydrogen energy is a clean and efficient new energy [3,4]. Therefore, the hydrogen production technology using catalysts to decompose water under visible light has received extensive attention from researchers, and research in this area has got tremendous achievements [5-7]. The catalyst plays a decisive role in the photocatalytic system [8]. Generally, semiconductor nanomaterials (such as TiO_2, CdS, etc. [9,10]) are used as photocatalysts, they absorb photon energy under visible light and excite photoelectrons to participate in the hydrogen evolution reduction reaction in water [11]. However, since Honda and Fujishima observed photocatalysis in 1972 [12], there are still some problems in the field of photocatalytic hydrogen evolution. For example, semiconductor materials have low utilization of sunlight, and electrons and holes are easy to reorganize, limit the development of photocatalysis [13].

Today, researchers in the field of photocatalysis have reported hundreds of semiconductor materials that can decompose water under visible light [14,15], among them, TiO_2, ZnO, Fe_2O_3 and other metal oxides [16-18] have received extensive attention in terms of photocatalytic hydrogen production due to their low cost and good stability. As a typical metal oxide, WO_3 is an ideal photocatalyst with a band gap (E_g) of 2.4-2.8 eV [19]. However, because the conduction band (CB) position of WO_3 is relatively positive, it has a poor reducing ability in the photocatalytic water decomposition reaction [20]. The smaller band gap also makes it easier for the electrons and holes inside to recombine, so pure WO_3 has poor catalytic activity under visible light [21]. Therefore, some researchers combined WO_3 with other materials to optimize the hydrogen production activity, such as WO_3/ZnCdS [22], WO_3/g-C_3N_4 [23], WO_3/$BiVO_4$ [24] and WO_3-CuS [25].

In recent years, transition metal sulfide (WS_2, NiS, MoS_2, Co_9S_8, CoS_2, etc.) [26] have shown excellent hydrogen production performance in the field of photocatalysis, and such semiconductor materials are cheap and readily available. The inherent metal conductivity of CoS_2 can accelerate the transfer of electrons. Therefore, CoS_2 has excellent catalytic activity in photocatalysis and electrocatalysis [27]. So far, CoS_2 has been extensively studied in the field of electrocatalysis, but relatively little research has been done on the production of H_2 by photocatalysis [28].

In this study, a simple hydrothermal method was used to load WO_3 on the surface of CoS_2 to synthesize a new photocatalytic composite material, which was first applied to photocatalytic hydrogen production. Experimental results illustrated that in the photocatalytic system with 10% triethanolamine solution (10% TEOA solution, pH=9) as electronic sacrificial agent and Eosin Y (EY) as sensitizer, the WCS-2 composite had higher H_2 evolution activity than pure WO_3 or CoS_2 single catalyst.

2.Experimental section

2.1 Materials

NaCl (Sodium chloride, 99.5%), $Na_2WO_4{\cdot}2H_2O$ (Sodium tungstate dihydrate, 99.5%), HCl (hydrochloric acid, 36-38%), $Co(NO_3)_2{\cdot}6H_2O$ (cobalt nitrate hexahydrate, 99.99%), $Na_2S_2O_3{\cdot}5H_2O$ (sodium thiosulfate, 99.5%), anhydrous ethanol (99.7%), and deionized water (DW) made by ultrapure water mahine.

2.2. Synthesis of WO_3

According to previous reports [19], using hydrochloric acid as a surfactant, WO_3 was prepared by hydrothermal method. Weigh 6.14 mmol $Na_2WO_4{\cdot}2H_2O$ and 12.70 mmol NaCl dissolved in deionized water of 50 mL, then put it on a magnetic stirrer and stirred for 1 h. Concentrated HCl (8 mL) was added dropwise during the stirring process, the solution gradually became pale-yellow. Later, the mixture was moved to a 100 mL polytetrafluoroethylene (PTFE) reaction still, kept at 180 ℃ for 24 h. After cooling, the products were washed 3 times with anhydrous ethanol and DW, and then dried in an oven for 8 h at 60 ℃.

2.3. Synthesis of CoS_2

4 mmol $Na_2S_2O_3{\cdot}5H_2O$ and 2 mmol $Co(NO_3)_2{\cdot}6H_2O$ were dissolved in a beaker containing 40 mL DW, and then added 30 mL of anhydrous ethanol, continuously stirred for 1 h. Then, the mixture was moved to a 100 mL PTFE reaction still and reacted for 12 h at 180 ℃. After cooling, the washing and drying process of CoS_2 was the same as that of WO_3.

2.4. Preparation of the WO_3/CoS_2

Added 100 mg CoS_2 and 55 mg, 58 mg, 60 mg, 62 mg or 65 mg WO_3 (WCS-1, WCS-2, WCS-3, WCS-4, WCS-5, respectively named) to a beaker filled with 50 mL of deionized water, sonicated for 20 min and stirred 1 h, transferred to 100 mL PTFE high-pressure reactor at 180 ℃ for 12 h. After natural cooling, washed and dried.

2.5. Characterizations

Advanced X-ray diffraction (Rigaku Smartlab, XRD) and Cu Kα radiation were used to determine the crystal texture of photocatalysts. Obtained SEM (scanning electron microscope) images of sample through ZEISS EVO 18 instrument. TEM and HRTEM (high-low magnification transmission electron microscopy, JEOL JEM-2100) were used to study morphology and lattice. X-ray photoelectron spectroscopy (XPS, ESCALAB 250Xi) was used to study the chemical states of the elements in WCS-2. The photoluminescence (PL) spectrum of the catalyst was obtained using a fluorescence spectrophotometer (fluoromax-4). With $BaSO_4$ as a background. UV-visible spectrophotometer (Lambda 750 S) was used to obtain the UV-visble diffuse reflection spectrum (UV-Vis DRS) of catalyst. A N_2 adsorption-desorption instrument (ASAP 2020 M) was used to detect the BET specific surface area (S_{BET}) and pore diameter distribution of the catalyst.

2.6. Photocatalytic activity assessment

The photocatalytic hydrogen production test was performed in a flat-bottomed quartz bottle (65 mL) with sealed rubber pad. A typical experimental procedure was to disperse the prepared 10 mg of catalyst powder in a quartz bottle including 30 mL of TEOA solution (10%, v/v, pH=9), and then added 16 mg EY, after stirred and sonicated to form a homogeneous solution. Filled with N_2 in anaerobic environment for 20 min to discharge other gases in the reaction bottle. Then put the reaction bottle into the multi-channel photocatalytic reaction system with 5W LED lamps for 5 h of hydrogen evolution experiment, and used gas chromatograph (SP-2100, TCD, 13X column, N_2 carrier) to detect the amount of H_2 precipitation.

2.7. Photoelectrochemical measurement

A standard three-electrode electrochemical workstation (VersaSTA4-400, AMETEK) was used for electrochemical testing of the photocatalyst. 0.2 mol/L Na_2SO_4 solution was used as electrolyte

solution, the counter electrode was Pt electrode and reference electrode was saturated calomel electrode (SCE). Working electrode: Dispersed 12 mg of sample powder in 1.5 mL of anhydrous ethanol and stirred until thick, and evenly coated it on ITO (conductive glass). The effective area was about one square centimeter. After drying, a working electrode was obtained. Under the condition of 0.5 V bias and 300 W Xe lamp (CEL-HXF300, $\lambda \geq 420$ nm) as a stable light source, electrochemical data were measured.

3.Results and discussion

3.1. XRD tests

Fig. 1 showed the XRD pictures of different photocatalysts synthesized. In Fig. 1a, the XRD diffraction peak of pure WO_3 was consistent with the data of WO_3 standard card (PDF#83-950). The diffraction peaks at 27.9°, 32.3°, 36.2°, 39.7°, 46.2°, and 54.9° correspond to the (111), (200), (210), (211), (220) and (311) crystal planes of CoS_2 (PDF#41-1471), respectively. Moreover, in the red curve (the XRD of WCS-2), both the diffraction peaks of WO_3 and CoS_2 existed and there was almost no change in the peak position. The above results indicated that pure WO_3, CoS_2 and WCS-2 composite catalysts were successfully synthesized. The XRD diffraction peaks of the WO_3/CoS_2 with different proportions prepared by changing the amount of WO_3 were shown in Fig. 1b, the difference in the intensity of diffraction peak may be due to the physical environment in the synthesis process. In addition, the XRD patterns of the WO_3/CoS_2 catalysts with different ratios had no other peaks except for the diffraction peaks of WO_3 and CoS_2, showing that the synthesized WO_3/CoS_2 had a relatively high purity.

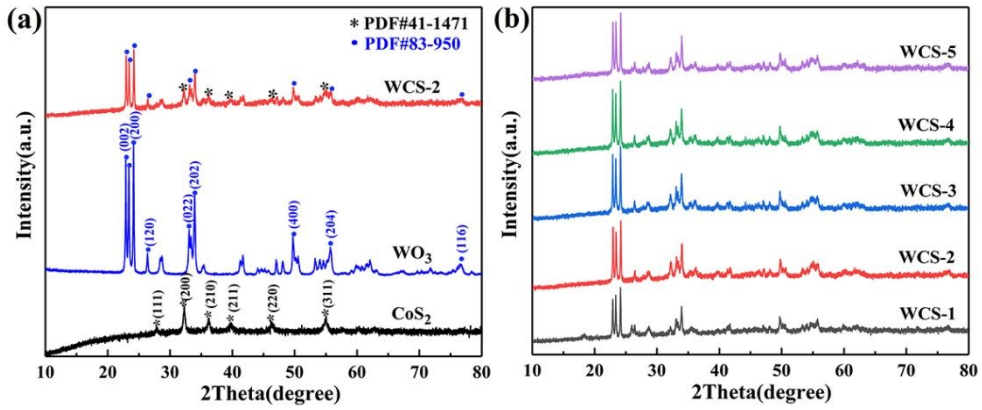

Fig. 1. XRD pattern: (a) WO_3, CoS_2, WCS-2 and (b) WO_3/CoS_2 with different proportions.

View Article Online
DOI: 10.1039/D0NJ04021E

3.2. Morphology and Structure Analysis

Fig. 2 was the SEM and TEM images of the sample. It could be found from Fig. 2a of SEM that CoS_2 existed as a spherical structure with irregular size, and the surface of the sphere was relatively smooth. The WO_3 sample (Fig. 2b) consisted of an irregular nano-block structure. Combined with XRD, the main reason for the irregular structure may be that WO_3 had poor crystallinity. As shown in SEM (Fig. 2c) and TEM (Fig. 2d) of the WCS-2 composite catalyst, because a large amount of WO_3 was uniformly and tightly dispersed on CoS_2 sphere, compared with the single CoS_2, the surface of WCS-2 composite catalyst was relatively rough, provided abundant active sites, and the close contact between WO_3 and CoS_2 facilitated charge transfer. The HRTEM of the WCS-2 composite catalyst was shown in Fig. 2e, the lattice fringe spacing of 0.361 and 0.242 nm, belong to the (200) crystal plane of WO_3 and the (210) plane of CoS_2, respectively. The energy dispersive X-ray (EDX) spectrum (Fig. 2f) showed that the WCS-2 composite material was composed of Co, O, S, W elements, and the elements were evenly distributed (Fig. 2g-k). This result indicated that WCS-2 was successfully synthesized.

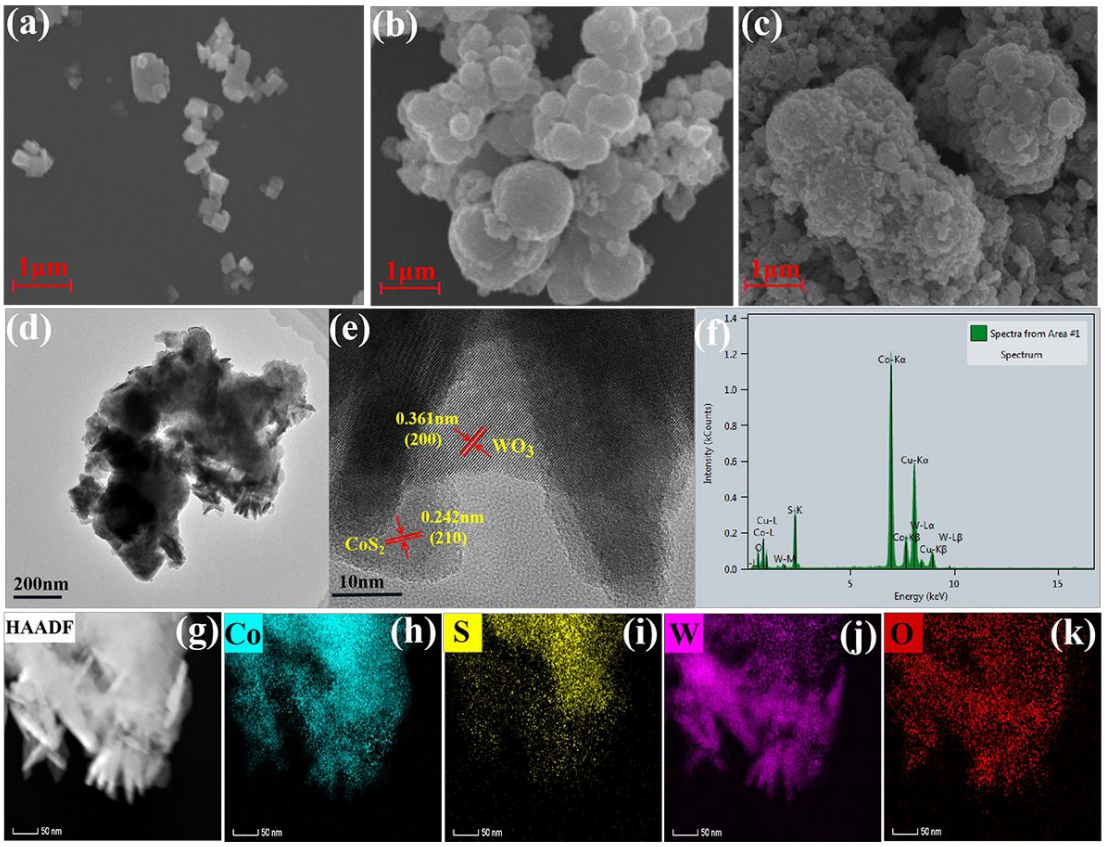

Fig. 2. SEM images of (a) WO_3, (b) CoS_2 and (c) WCS-2. (d) TEM, (e) HRTEM, and (f) EDX spectrum of WCS-2. (g-k) elemental mapping of WCS-2.

3.3. XPS studies

The elemental valence-state of WCS-2 composite catalyst was analyzed by XPS. In the full spectrum (Fig. 3e), W, O, S and Co elements were included into the WCS-2. As shown in Fig. 3a, the XPS of Co 2p can be fitted to four peaks, the two peaks located at the binding energy of 798.1 eV and 781.9 eV can be attributed to Co $2p_{1/2}$ and Co $2p_{3/2}$, resprctively. And at the binding energy of 803.9 eV and 786.7 eV were satellite peaks of Co^{2+} [29]. In Fig. 3b, the peaks of S 2p spectrum at 168.6 eV and 169.7 eV corresponded to S $2p_{3/2}$ and S $2p_{1/2}$ [30]. In Fig. 3c, the peaks at 37.8 eV and 35.6 eV corresponded to W $4f_{5/2}$ and W $4f_{7/2}$ respectively, indicated that element W in the composite catalyst existed as W^{6+} [31]. Fig. 3d showed that O 1s had only one peak at 531.8 eV, which can be attributed to the O^{2-} ions in WO_3 [32].

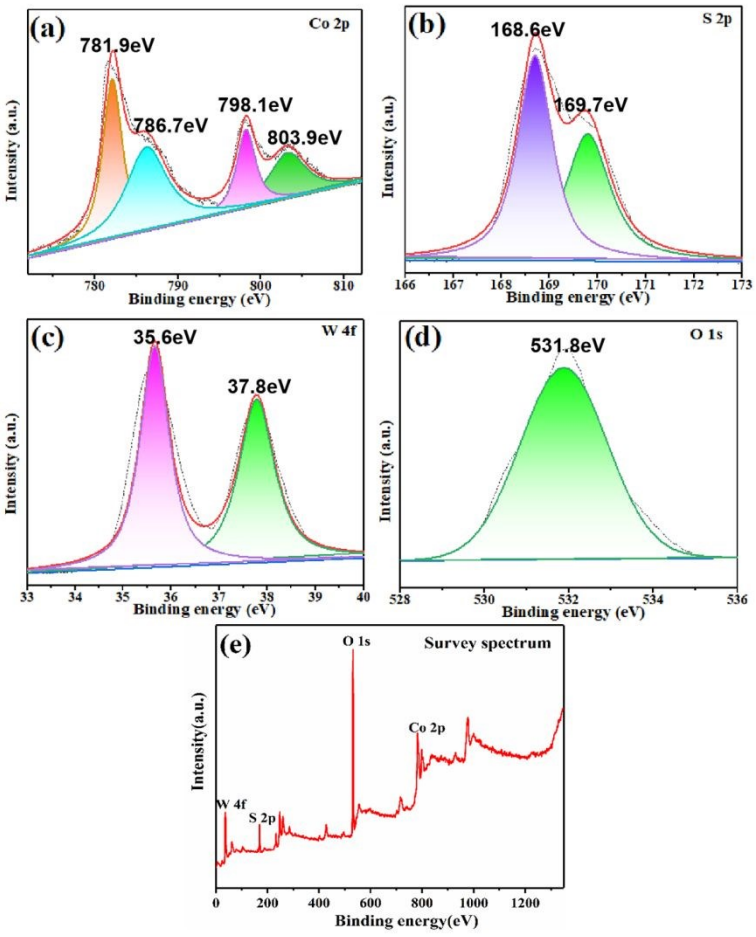

Fig. 3. XPS analysis of WCS-2: (a)Co 2p, (b)S 2p, (c)W 4f, (d)O 1s and (e) Survey spectrum.

View Article Online
DOI: 10.1039/D0NJ04021E

3.4. UV-Vis DRS

In order to analyze the optical performance of the catalyst, the UV-Vis DRS of the WO_3, CoS_2 and WCS-X (X=1,2,3,4,5) samples were studied. The results were shown in Fig. 4a (the inset was a partial enlargement between 250nm and 500nm). The CoS_2 sample had the highest light absorption intensity, and the light absorption edge of the WO_3 sample appeared at about 460 nm, and the wavelength between 460-800 nm light response intensity was lower. Compared with the pure WO_3 sample, the light absorption intensity of the composite material was obviously increased, especially between 400-800nm, which further showed that the WO_3 catalyst had been successfully loaded on the CoS_2 surface. The light absorption intensity of WCS-2 was significantly higher than other composite materials, and it had a more excellent light absorption performance in the visible light range. When the load was too large, the agglomeration state of WO_3 will appear again, which was not conducive to the response to light. In addition, according to the equation: $\alpha h\nu=A(h\nu-Eg)^n$ (n is 2 or 1/2, $h\nu$ is the photon energy, α is the absorption coefficient) [33], the data of the UV-visible diffuse reflection can be processed to obtain Fig. 4b-d, where the intersection of the tangent and the x-axis was the E_g of the catalyst. It could be seen that the E_g of WO_3, CoS_2 and WCS-2 were 2.41, 2.14 and 2.04 eV, respectively. Compared with the other two pure substances, the E_g of the WCS-2 photocatalyst was reduced. Moreover, the light absorption edge of WCS-2 showed a clear red shift compared to WO_3. These results indicated that the synergy between WO_3 and CoS_2 can improve the utilization of visible light.

View Article Online
DOI: 10.1039/D0NJ04021E

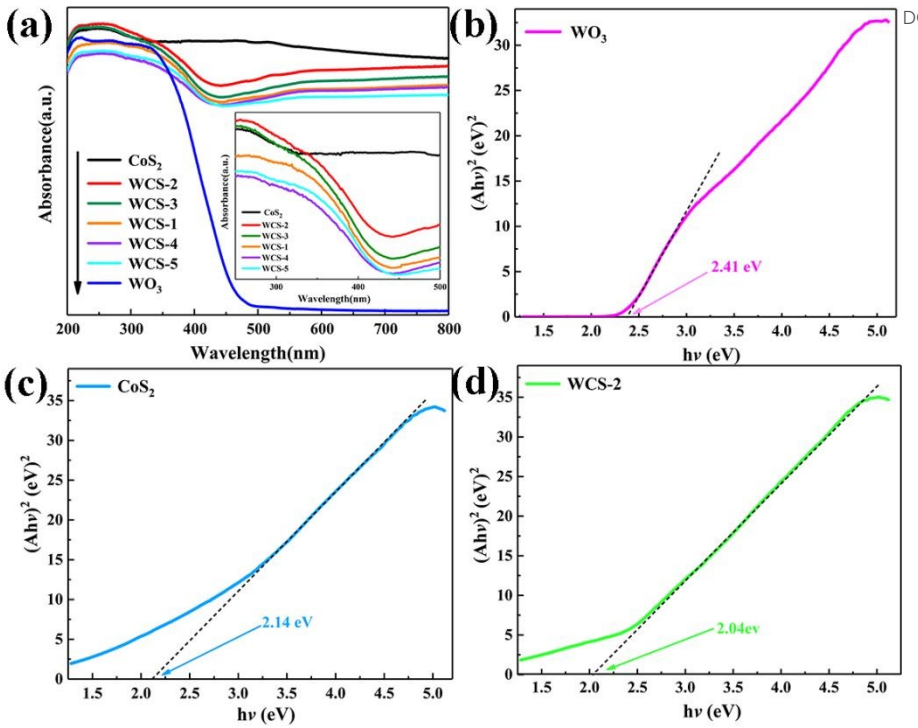

Fig. 4. (a) UV-Vis DRS of all samples; (b) E_g of WO_3, (c) CoS_2, and (d) WCS-2.

3.5. BET Analysis

The N_2 adsorption-desorption isotherms and pore diameter distributions of WO_3, CoS_2 and WCS-2 were shown in Fig. 5. As shown in Fig. 5a, three photocatalysts were type IV isotherms with H3 hysteresis loop, which indicated that all the three samples were mesoporous materials. As shown in Fig. 5b, the pore size of the three catalysts was concentrated at 2-50 nm, and also from Table 1, the average pore size of WO_3, CoS_2 and WCS-2 were 11, 12 and 15 nm respectively, further illustrating the sample all were mesoporous materials. In addition, it can be found from Table 1 that the S_{BET} of WCS-2 was 14.83 m^2/g, which was significantly higher than that of WO_3 (9.24 m^2/g) and CoS_2 (7.54 m^2/g). This might be due to the fact that the agglomerated state of WO_3 was broken after being compounded with CoS_2 and uniformly dispersed on the surface of the CoS_2 spherical particles. Similarly, WCS-2 had the largest pore volume. For WCS-2 complex catalyst, a larger S_{BET} could provide more active sites, which might be beneficial to photocatalytic reactions.

View Article Online
DOI: 10.1039/D0NJ04021E

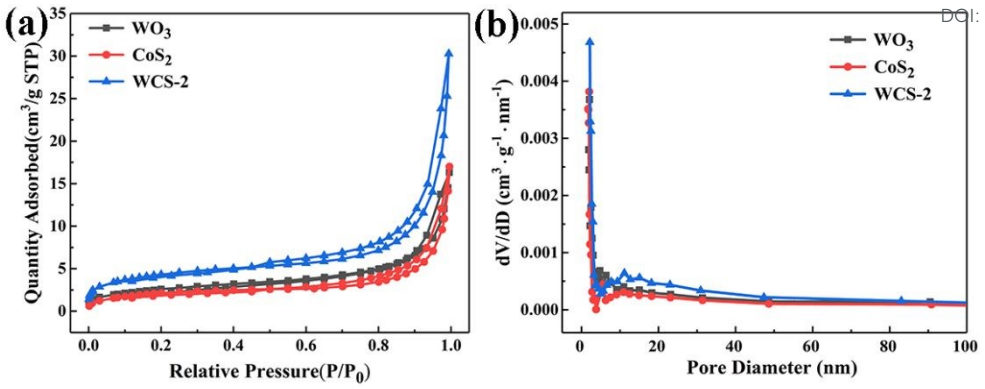

Fig. 5. (a) N_2 adsorption-desorption isotherm, (b) pore diameter distribution curves of WO_3, CoS_2 and WCS-2.

Table 1. The S_{BET}, pore volume (P-V) and pore size (P-S) for three catalyst.

Catalyst	S_{BET}(m^2/g)	P-V (cm^3/g)	P-S (nm)
WO_3	9.238	0.025	11.013
CoS_2	7.540	0.026	15.014
WCS-2	14.828	0.048	12.103

3.6. PL analysis

The hole-electrons separation efficiency in the catalyst can be analyzed by the quenching of fluorescence in the PL spectrum. Generally, the better the photocatalytic activity of catalyst, the lower the steady-state fluorescence intensity and the higher the hole-electrons separation efficiency. The PL spectra of all samples were shown in Fig. 6, in TEOA solution (10%, pH=9), and under a 480 nm excitation wavelength, the highest emission peak with a peak intensity of 537 nm appeared in the presence of EY alone. After adding WO_3 or CoS_2 single catalyst to the solution, the peak intensity of PL decreased slightly. However, when WO_3 was introduced on the surface of CoS_2 catalyst, the peak intensity of various composite catalysts was obviously weakened, indicating that the prepared composite material, especially WCS-2, had better fluorescence quenching effect than single catalyst. However, the peak intensity of WCS-3, 4, and 5 was higher than that of WCS-2. This may be because after loading excessive WO_3, a new electron-hole recombination center was formed between WO_3 and CoS_2. The results showed that

the formation of n-n heterojunction between WO_3 and CoS_2 effectively inhibited the electron and hole recombination, promoted the photogenic electron transfer. Therefore, it was beneficial to improve the H_2 evolution activity of the photocatalyst.

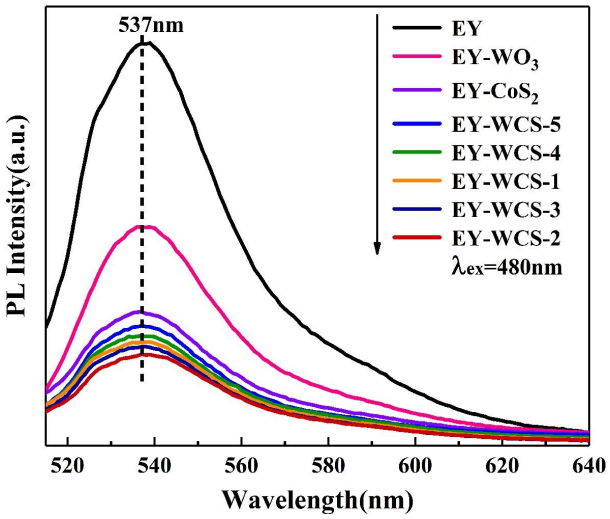

Fig. 6. Steady-state fluorescence of all samples.

3.7. Hydrogen production experiment

For researching the photocatalytic activity of the prepared WO_3/CoS_2, in Fig. 7a-b, the H_2 evolution of different catalysts under the same conditions were compared. As shown in Fig. 7a, hydrogen evolution of pure WO_3 and CoS_2 at the fifth hour was 2.75 μmol and 101.97 μmol, respectively. The WCS-2 composite catalyst produced the highest amount of hydrogen, reaching 221.15 μmol in the fifth hour, which was 80.41 times that of WO_3 and 2.17 times that of CoS_2 under the same conditions. The WCS-2 had excellent hydrogen evolution property, which was related to a good synergy between WO_3 and CoS_2. It can be seen from Fig. 7b that when the amount of CoS_2 was fixed, the loading of WO_3 with different qualities had a significant influence on the H_2 evolution activity of the WO_3/CoS_2 catalyst. Compared with pure CoS_2, with increasing WO_3 loadings, hydrogen evolution had a tendency to increase first and then decrease. This may be because the surface of CoS_2 changes from smooth to rough after loading an appropriate amount of WO_3. This defect could be used as a center for trapping electrons, which facilitated the separation of electrons and holes. And excessive WO_3 was loaded on the CoS_2 surface, which masked the active site of material, thereby reducing the hydrogen evolution activity. Compared with other composite catalysts containing WO_3 or CoS_2, WCS-2 had better H_2 production performance. The

View Article Online
DOI: 10.1039/D0NJ04021E

comparison results were shown in Table 2.

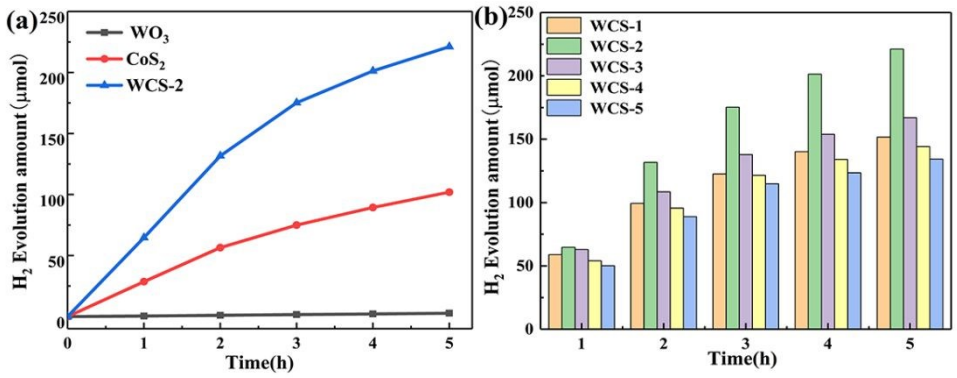

Fig. 7. Photocatalytic hydrogen evolution comparison of (a)WO_3, CoS_2, WCS-2, and (b) WCS-X (X=1, 2, 3, 4, 5).

Table 2. Comparison of the hydrogen production activity of WO_3/CoS_2 and similar photocatalysts previously reported.

Photocatalyst	Light source	Sacrificial reagent	Activity (μmol/g·h)	Ref.
WO_3/CoS_2	5 W LED ($\lambda \geq 420$ nm)	10 vol% TEOA	4423	This work
WO_3@$ZnIn_2S$	300 W Xe-lamp ($\lambda \geq 420$ nm)	15 vol% TEOA	3900	[21]
WO_3/ZnCdS	105 W LED ($\lambda \geq 450$ nm)	20 vol% lactic acid	10990	[22]
NiS/WO_3/g-C_3N_4	5 W LED ($\lambda \geq 420$ nm)	15 vol% TEOA	2929	[34]
CdS/(WO_3&WS_2)	300 W Xe-lamp ($\lambda \geq 400$ nm)	10 vol% lactic acid	754	[35]
WS_2/WO_3	300 W Xe-lamp (without filter)	10 vol% lactic acid	680	[36]
TiO_2/WO_3/Pt	300 W Xe-lamp	45mL H_2O + 25mL CH_3OH	129	[37]

View Article Online
DOI: 10.1039/D0NJ04021E

	(without filter)			
CoS_2/g-C_3N_4	300 W Xe-lamp ($\lambda \geq 420$ nm)	10 vol% TEOA	578	[38]
CoS_2/$FeLaO_3$	5 W LED ($\lambda \geq 420$ nm)	10 vol% TEOA	5594	[39]

In previous reports, the hydrogen evolution activity of the semiconductor catalyst in EY-sensitized system was affected by pH and the quality of EY. Therefore, the pH of 10 % TEOA solution was adjusted or the mass of EY was changed during WCS-2 photocatalytic hydrogen production experiment. As shown in Fig. 8a, when pH=9, the WCS-2 material had the best hydrogen production performance. As the pH value increased, hydrogen production gradually decreased. This was because in a more alkaline solution, the consistence of H^+ was low, the driving force for H_2 production was suppressed, thereby reducing the H_2 evolution activity of the catalyst. And when the pH was relatively low, there were too many H^+, the solution may be protonated, and reduced electronic supply capacity, thereby reducing the efficiency of exciting EY molecules [40].

In Fig. 8b, the hydrogen production effect was the best when added 16 mg EY. The hydrogen production of WCS-2 tended to increase first and then reduce as the mass of EY increases. Because increasing the amount of EY was beneficial for the catalyst to adsorb dye on the surface and accelerated electron transfer, but excessive addition of EY would cause free EY molecules to absorb the incident light, reducing the utilization rate of the catalyst to the light source, thereby reducing the photocatalytic performance [39].

Fig. 8c was a 20 h stability test of WCS-2 composite catalyst. The WCS-2 had the best hydrogen evolution property, in the first cycle. In contrast, the H_2 evolution of the second and fourth cycles was markedly reduced, and before the third cycle, 3 mg EY was added, and the H_2 evolution was the same as the second. Compared with the circulation, there was a recovery, which may be caused by the loss of part of the catalyst during centrifugation, and the prolonged light

decomposition of EY. Fig. 8d tested the XRD patterns of the WCS-2 before and after the photocatalytic experiment. The XRD before and after hydrogen production did not change significantly, showing that the crystalline phase structure of WCS-2 did not change after the experiment. The results showed that the photocatalytic property of WCS-2 composite material was comparatively stable.

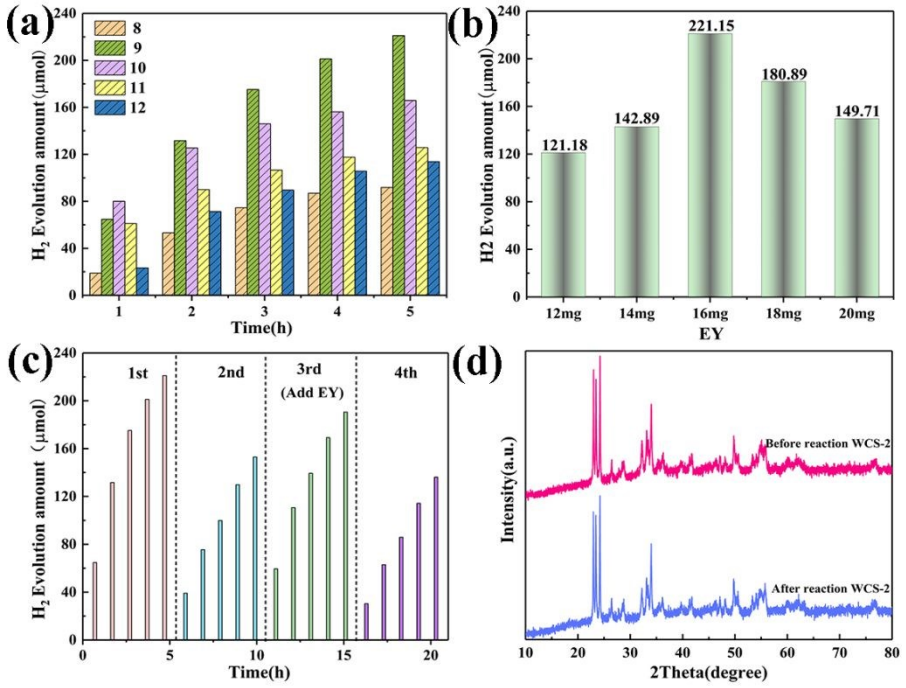

Fig. 8. (a) Optimize PH (b) Adjust EY concentration (c) Stability test (d) XRD pattern before and after hydrogen production by WCS-2.

3.8. Photoelectrochemical experiment

To learn more about the electron transfer mechanism of WCS-2 composite material, the following electrochemical tests were carried out. From the results of transient photocurrent of WO_3, CoS_2 and WCS-2 samples (Fig. 9a), it can be seen that under the action of four visible light ($\lambda \geq 420$nm) switching cycles, there were photocurrent response curves (I-T curve), and all the photocurrent response were uniform. It explained that WO_3, CoS_2 and WCS-X can all be used as an excellent photocatalyst. Compared with the two single photocatalysts, the WCS-2 catalyst had the highest photocurrent intensity, which indicated that under visible light, WCS-2 samples had faster electron and hole transfer speeds and lower recombination rates. Moreover, the photocurrent

intensity trend of other composite catalysts was consistent with the hydrogen production activity. This showed that loading an appropriate amount of WO_3 can effectively promote the separation of photogenerated carriers and improve the activity of hydrogen production.

The photocatalytic activity depends highly on the over-potential of the photocatalytic reaction [41], so the linear scanning voltammetry (LSV) curves of WO_3, CoS_2 and WCS-X samples were tested. It can be found from Fig. 9b, under the same voltage conditions, the overpotential of each composite catalyst was lower than that of two single catalysts. Among them, the over-potential of the WCS-2 sample was the lowest, indicating that the photocatalytic activity of WCS-2 was the best, which was consistent with the hydrogen evolution activity, and can indicate that WCS-2 was an excellent photocatalytic material.

Fig. 9c showed the electrochemical impedance spectroscopy (EIS) of WO_3, CoS_2 and WCS-X. The radius of curvature reflected the magnitude of the resistance received during charge transfer. A small arc radius indicated fast charge transfer. In Fig. 9c, the arc radius of each composite catalyst was significantly reduced after WO_3 was doped, indicating that the introduction of WO_3 could accelerate the transfer of electrons, thereby improving the photocatalytic activity. In particular, WCS-2 had the smallest arc radius, which means that the electrons in WCS-2 had the least resistance and the fastest electron transfer.

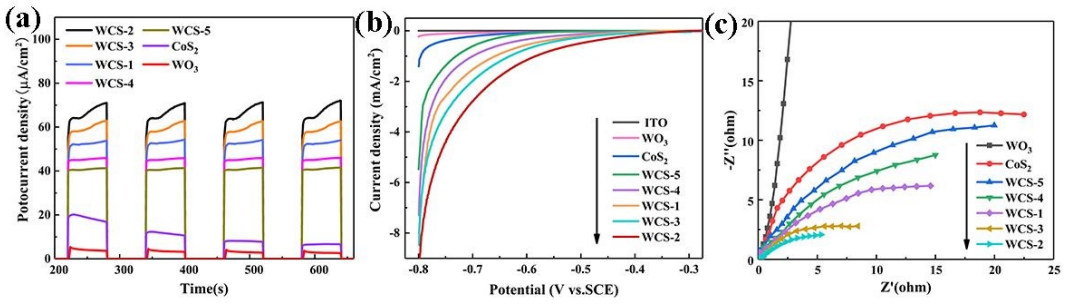

Fig. 9. (a) I-T, (b) LSV and (c) EIS curves of the prepared sample in 0.2 M Na_2SO_4 solution.

The flat band potential (E_{fb}) of a single catalyst was tested using Mott-Schottky (M-S) curve [42]. As shown in Fig. 10a and 10b, it can be seen from the positive slope of the curves that both WO_3 and CoS_2 were n-type semiconductors [43], and measured against SCE, the E_{fb} of WO_3 and CoS_2 were approximately 0.56 V and -0.53 V. Generally, the E_{fb} of a n-type semiconductor is 0.2

V or 0.1 V lower than the E_{CB} potential. Consequently, relative to SCE, the E_{CB} of WO_3 and CoS_2 can be estimated as 0.36 V and -0.73 V, then used $E_{NHE}=E_{SCE}+0.241$ V [44] formula to correct it to the value under the NHE (normal hydrogen electrode), the E_{CB} of WO_3 was 0.60 V and the E_{CB} of CoS_2 was -0.49 V. Finally, used the formula $E_{VB}=E_{CB}+E_g$ combined with E_g (Fig. 4b and 4c, WO_3 was 2.41 eV, CoS_2 was 2.14 eV), calculated the WO_3 and CoS_2 valence band (E_{VB}) were 3.01 V, 1.65 V.

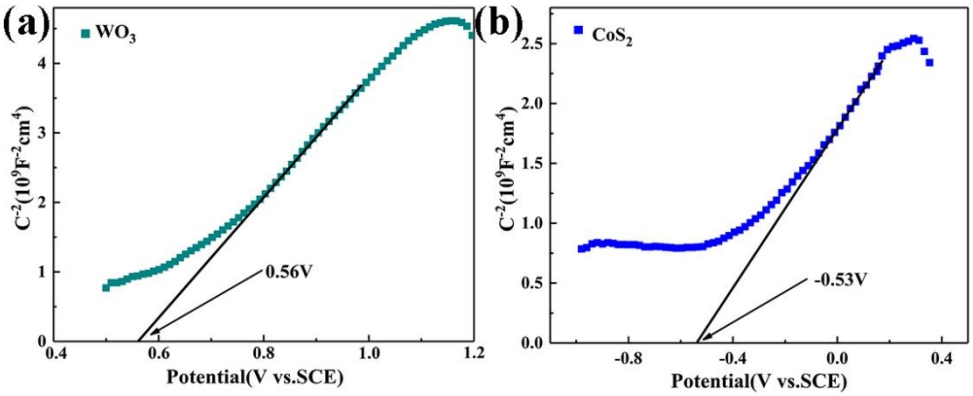

Fig. 10. M-S plots of (a) WO_3 and (b) CoS_2.

3.9. Photocatalytic reaction mechanism

Based on the above results, it was speculated that the photocatalytic mechanism of WCS-2 material in the EY system. After the light irradiation (Fig. 11), the EY adsorbed on WCS-2 formed the singlet excited state EY^{1}*. Then through a system transition, EY^{1}* became a triplet excited state EY^{3}*. TEOA provided electrons to quench and reduce EY^{3}* to EY^{-}*. Electrons of EY^{-}* were further moved to the surface of WCS-2 and restored to EY due to the loss of electrons. Electrons on the surface of the WCS-2 sample reacted with H^+ in TEOA solution to generate hydrogen. Meanwhile, after absorbing photons, WO_3 and CoS_2 both generated electrons and removed from the VB to the CB, leaving holes in the VB. At this time, if it was a traditional type II heterojunction (Fig. 11a), electrons in the CB of CoS_2 would moved to the CB of WO_3. However, these electrons in the CB of WO_3 were not conducive to the reduction of H_2O to H_2, the reason was that the standard redox potential of H^+/H_2 (0.00 eV vs. NHE) was more negative than the conduction band potential of WO_3 (0.60eV vs. NHE), which was in agreement with the previous H_2 evolution results of WO_3 single catalyst. Therefore, the electron transfer mechanism of type II

heterojunction was negated. In addition, the Z-scheme electron transfer mechanism was shown in Fig. 11b, electrons in the CB of WO_3 were moved to the VB of CoS_2 to combine with the holes, and the electrons in the CB of CoS_2 reduced protons to H_2, and the holes in the valence band of WO_3 were depleted by the TEOA. This mechanism of Z-scheme effectively promoted the photocarrier transfer of the WCS-2 and enhanced the photocatalytic hydrogen production activity, which was in line with the experimental results of WCS-2 with higher hydrogen evolution activity than the single photocatalyst. Therefore, it can be seen that WO_3/CoS_2 n-n heterojunction may follow the Z-scheme system.

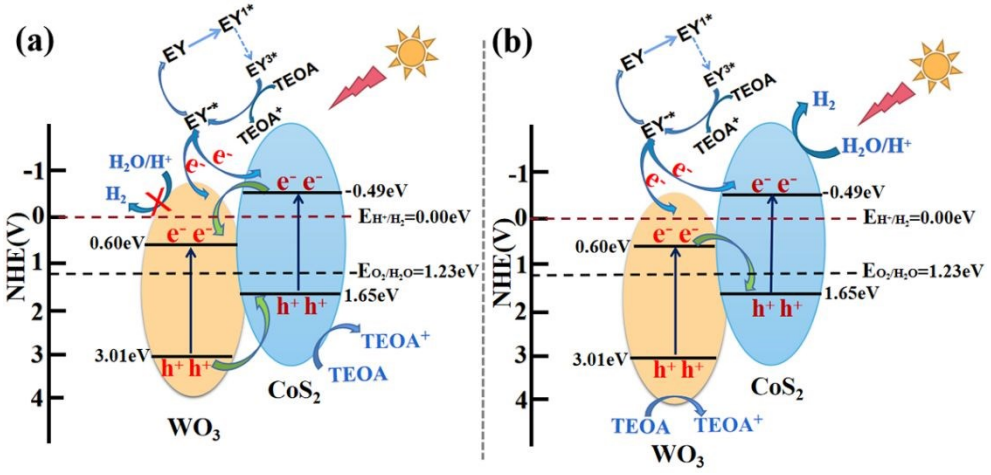

Fig. 11. The mechanism of WO_3/CoS_2 n-n heterojunction decomposing water under visible light was speculated: (a)Type II heterojunction, (b) Z-scheme system.

4. Conclusion

In summary, it was proved that the hydrothermal method had successfully synthesized the WO_3/CoS_2 composite material. After WO_3 was supported on the CoS_2 surface, the catalyst surface became rough and the specific surface area increased, which not only enhanced the adsorption capacity of EY molecules but also provided multiple active sites. Compared with pure WO_3 and CoS_2, WO_3/CoS_2 had excellent photocatalytic H_2 evolution performance, and it can be known from the hydrogen production experiment that the loading of WO_3 had a large influence on the H_2 evolution performance of the WO_3/CoS_2. Among them, the sample (WCS-2) synthesized with 58 mg WO_3 and 100 mg CoS_2 had the best hydrogen production performance. In addition, from steady-state fluorescence and electrochemical tests (I-T, LSV, EIS), it was known that the

heterojunction formed at the interface of the composite material suppresses the recombination of photoelectrons and holes, and facilitated electron transfer. This work showed that the WO_3/CoS_2 composite material of the Z-scheme system was a stable new photocatalyst.

Conflicts of interest

There are no conflicts to declare.

Acknowledgements

This work was financially supported by Xixia District Science and Technology Plan Project (XXKJ1901). This work also was supported by the New Catalytic Process in Clean Energy Production (ZDZX201803), and the Natural Science Foundation of Ningxia Province (NZ17262).

References

[1] B. Liu, S. X. Liu, S. S. Guo, S. X. Zhang, Economic study of a large-scale renewable hydrogen application utilizing surplus renewable energy and natural gas pipeline transportation in China, *Int. J. Hydrogen Energy*, 45(2020), 1385-1398.

[2] R. G. Li, Latest progress in hydrogen production from solar water splitting via photocatalysis, photoelectrochemical, and photovoltaic-photoelectrochemical solutions, *Chin J. Catal.* , 38(2017), 5-12.

[3] F. Dawood, M. Anda, G. M. Shafiullah, Hydrogen production for energy: An overview, *Int. J. Hydrogen Energy*, 45(2020), 3847-3869.

[4] G. Y. Liu, Y. Sheng, J. W. Ager, M. Kraft, R. Xu, Research advances towards large-scale solar hydrogen production from water, *EnergyChem*, 1(2019), 100014.

[5] G. Colón, Towards the hydrogen production by photocatalysis, *Appl. Catal. A*, 518(2016), 48-59.

[6] A. Fujishima, K. Honda, Electrochemical photolysis of water at a semiconductor electrode, *Nature*, 238 (1972), 37-38.

[7] K. Fan, Z. L. Jin, G. R. Wang, H. Yang, D. D. Liu, et al., Distinctive organized molecular assemble of MoS_2, MOF and Co_3O_4, for efficient dye-sensitized photocatalytic H_2 evolution, *Catal .Sci. Technol.*, 8(2018), 2352-2363.

[8] Y. Peng, G. Han, D. Wang, K. X. Wang, Z. N. Guo, Improved H_2 evolution under visible light in heterostructured SiC/CdS photocatalyst: Effect of lattice match, *Int. J. Hydrogen Energy*, 42 (2017), 14409-14417.

[9] G. Liu, L. Yin, J. Wang, P. Niu, C. Zhen, Y. Xie, et al., A red anatase TiO_2 photocatalyst for solar energy conversion, *Energy Environ. Sci.*, 5 (2012), 9603-9610.

[10] S. A. Pawar, D. S. Patil, A. C. Lokhande, M. G. Gang, J. C. Shin, et al., Chemical synthesis of CdS onto TiO_2 nanorods for quantum dot sensitized solar cells, *Opt. Mater.*, 58(2016), 46-50.

[11] L. L. Zhang, H.W.Zhang, C. K. Jiang, J. Yuan, X. Y.Huang, et al., Z-scheme system of WO_3@MoS_2/CdS for photocatalytic evolution H_2: MoS_2 as the charge transfer mode switcher, electron-hole mediator and cocatalyst, *Appl. Catal. B: Environ.*, 259(2019), 118073.

[12] A. Fujishima, K. Honda, Electrochemical photolysis of water at a semiconductor electrode, *Nature*, 238 (1972), 37.

[13] S. Zhao, J. Xu, Z. T. Li, Z. Y. Liu, Y. R. Li, Molybdenum disulfide coated nickel-cobalt sulfide with nickel phosphide loading to build hollow core-shell structure for highly efficient photocatalytic hydrogen evolution, *J. Colloid Interface Sci.*, 555(2019), 689-701.

[14] M. B. Tahir, G. Nabi, T. Iqbal, M. Sagir, M. Rafique, Role of $MoSe_2$ on nanostructures WO_3-CNT performance for photocatalytic hydrogen evolution, *Ceram. Int.*, 44(2018), 6686-6690.

[15] J. Theerthagiri, R. A. Senthil, A. Malathi, A. Selvi, J. Madhavan, M. Ashokkumar, Synthesis and characterization of a CuS-WO_3 composite photocatalyst for enhanced visible light photocatalytic activity, *RSC Advances*, 5(2015), 52718-52725.

[16] A. K. L. Sajjad, S. Shamaila, B. Tian, F. Chen, J. Zhang, One step activation of WO_x/TiO_2 nanocomposites with enhanced photocatalytic activity, *Appl. Catal. B: Environ.*, 91(2009), 397-405.

[17] S. J. Darzi, A. R. Mahjoub, Investigation of phase transformation and photocatalytic properties of sol-gel prepare nanostructured ZnO/TiO_2 composites, *J. Alloys Compd.*, 486 (2009), 805-808.

[18] H. Kim, J. Kim, W. Kim, W. Choi, Enhanced photocatalytic and photoelectrochemical activity in the ternary hybrid of CdS/TiO_2/WO_3 through the cascadal electron transfer, *J.Phys. Chem. C*, 115 (2011), 9797-9805.

[19] M. B. Tahir, M. Sagir, N. Abas, Enhanced photocatalytic performance of CdO-WO_3 composite for hydrogen production, *Int. J. Hydrogen Energy*, 44(2019), 24690-24697.

[20] R. Adhikari, G. Gyawali, T. Sekino, S. W. Lee, Microwave assisted hydrothermal synthesis of Ag/AgCl/WO_3 photocatalyst and its photocatalytic activity under simulated solar light, *J. Solid State Chem.*, 197 (2013), 560-565.

[21] L. Ye, Z. H. Wen, $ZnIn_2S_4$ nanosheets decorating WO_3 nanorods core-shell hybrids for boosting visible-light photocatalysis hydrogen generation, *Int. J. Hydrogen Energy*, 44(2019), 3751-3759.

[22] L. M. Song, D. Liu, S. J. Zhang, J. F. Wei, WO_3 cocatalyst improves hydrogen evolution capacity of ZnCdS under visible light irradiation, *Int. J. Hydrogen Energy*, 44(2019), 16327-16335.

[23] L. Cui, X. Ding, Y. Wang, H. Shi, L. Huang, Y. Zuo, et al., Facile preparation of Z-scheme WO_3/g-C_3N_4 composite photocatalyst with enhanced photocatalytic performance under visible light, *Appl. Surf. Sci.*, 391(2017), 202-210.

[24] J. Z. Su, L. J. Guo, N. Z. Bao, C. A. Grimes, Nanostructured WO_3/$BiVO_4$ heterojunction films for efficient photoelectrochemical water splitting, *Nano Lett.*, 11(2011), 1928-1933.

[25] Y. T. Liu, M. Li, Q. Y. Zhang, P. C. Qin, X. D. Wang, et al., One-step synthesis of a WO_3-CuS nanosheet heterojunction with enhanced photocatalytic performance for methylene blue degradation and Cr(VI) reduction, *J. Chem. Technol. Biotechnol.*, 95(2020), 665-674.

[26] J. Tang, B. Gao, J. B. Pan, L. Chen, Z. H. Zhao, et al., CdS nanorods anchored with CoS_2 nanoparticles for enhanced photocatalytic hydrogen production, *Appl. Catal. A*, 588(2019), 117281.

[27] Y. Zhu, L. F. Song, N. Song, M. X. Li, C. Wang, X. F. Lu, Bifunctional and Efficient CoS_2-C@MoS_2 Core-Shell Nanofiber Electrocatalyst for Water Splitting, *ACS Sustain. Chem. Eng.*, 7(2019), 2899-2905.

[28] M. R. Gao, Y. R. Zheng, J. Jiang, S. H. Yu, Pyrite-type nanomaterials for advanced electrocatalysis, *Acc. Chem. Res.*, 50 (2017), 2194-2204.

[29] R. A. Senthil, Y. L. Wang, S. Osman, J. Q. Pan, Y. J. Lin, et al., A facile one-pot synthesis of microspherical-shaped CoS_2/CNT composite as Pt-free electrocatalyst for efficient hydrogen evolution reaction, *Int. J. Hydrogen Energy*, 44(2019), 16537-16547.

[30] D. Wang, J. Z. Liu, M. Zhang, Y. T. Song, Z. H. Zhang, et al., Construction of ternary annular 2Z-scheme+1Heterojunction CuO/WO_3/CdS/ photocatalytic system for methylene blue degradation with simultaneous hydrogen production, *Appl. Surf. Sci.*, 498(2019), 143843.

[31] L. J. Li, J. Xu, M. Mao, X. H. Li, S. Zhao, Z. Y. Liu, Y. R. Li, Effect of visible light irradiation on hydrogen production by $CoNi_2S_4$/$CdWO_4$ controllable flower spherical photocatalyst, *Appl. Surf. Sci.*, 481(2019), 692-701.

[32] G. Li， J. J. Hou, W. L. Zhang, P. W. Li,G. H. Liu, et al., Graphene-bridged WO_3/MoS_2 Z-scheme photocatalyst for enhanced photodegradation under visible light irradiation, *Mater. Chem. Phys.,* 246(2020), 122827.

[33] L. J. Li, J. Xu, J. P. Ma, Z. Y. Liu, Y. R. Li, A bimetallic sulfide $CuCo_2S_4$ with good synergistic effect was constructed to drive high performance photocatalytic hydrogen evolution, *J. Colloid Interf. Sci.*, 552(2019), 17-26.

[34] L. J. Zhang, X. Q. Hao, Y. B. Li, Z. L. Jin, Performance of WO_3/g-C_3N_4 heterojunction composite boosting with NiS for photocatalytic hydrogen evolution, *Appl. Surf. Sci.*, 499(2020), 143862.

[35] H. M. Wang, C. H. Li, L. Ying, P. F. Fang, WO_3&WS_2 nanorods coupled with CdS nanoparticles for enhanced visible light driven hydrogen evolution, *Appl. Surf. Sci.*, 448(2018), 539-546.

[36] S. Zhang, S. T. Chen, D. Liu, J. Zhang, T. Y. Peng, Layered WS_2/WO_3 Z-scheme photocatalyst constructed via an in situ sulfurization of hydrous WO_3 nanoplates for efficient H_2 generation, *Appl. Surf. Sci.*, 529(2020), 147013.

[37] H. Q. Gao, P. Zhang, J. H. Hu, J. M. Pan, J. J. Fan, G. S. Shao, One-dimensional Z-scheme TiO_2/WO_3/Pt heterostructures for enhanced hydrogen generation, *Appl. Surf . Sci.*, 391(2017), 211-217.

[38] Y. Z. Zhang, J. W. Shi, Z. X. Huang, X. J. Guan, S. C. Zong, et al., Synchronous construction of CoS_2 in-situ loading and S doping for g-C_3N_4: Enhanced photocatalytic H_2-evolution activity and mechanism insight, *Chem. Eng. J.*, 401(2020), 126135.

[39] L. j. Li, J. Xu, Rare earth perovskite modified cobalt disulfide catalysts controlled by reaction solvent synthesis to form a p-n heterojunction, *Appl. Surf. Sci.*, 505(2020), 143937.

[40] L. J. Zhang, G. R. Wang, X. Q. Hao, Z. L. Jin, Y. B. Wang, MOFs-derived Cu_3P@CoP p-n heterojunction for enhanced photocatalytic hydrogen evolution, *Chem. Eng. J.*, 395(2020), 125113.

[41]X. Hao, Z. Cui, J. Zhou, Y. Wang, Y. Hu, Y. Wang, Z. Zou, Architecture of high efficient zinc vacancy mediated Z-scheme photocatalyst from metal-organic frameworks, *Nano Energy*, 52 (2018), 105-116.

[42] J. L. Zhou, Z. Q. Zhang, X. L. Kong, F. He, R. X. Zhao, et al., A novel P-N heterojunction with staggered energy level based on $ZnFe_2O_4$ decorating SnS_2 nanosheet for efficient photocatalytic degradation, *Appl. Surf. Sci.*, 510(2020), 145442.

[43] Q. N. Wu, Q. J. Bu, S. Li, Y. H. Lin,X. X. Zou, et al., Enhanced interface charge transfer via n-n WO_3/Ti-Fe_2O_3 heterojunction formation for water splitting, *J. Alloys Compd.*, 803(2019), 1105-1111.

[44] Z. L. Jin, X. Yan, X. Q. Hao, Rational design of a novel p-n heterojunction based on 3D layered nanoflower MoSx supported $CoWO_4$ nanoparticles for superior photocatalytic hydrogen generation, *J. Colloid Interface Sci.*, 569(2020), 34-49.

View Article Online
DOI: 10.1039/D0NJ04021E

Table of contents entry

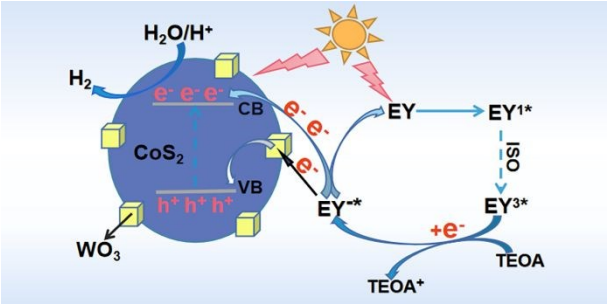

WO_3 and CoS_2 form n-n heterojunctions, and the synergy between them provides a new hydrogen-producing active center for each.